Uncooled Photodetector at Short-Wavelength Infrared Using InAs Nanowire Photoabsorbers on InP with P-N Heterojunctions

Dingkun Ren,[*†] Xiao Meng,[‡] Zixuan Rong,[†] Minh Cao,[†] Alan C. Farrell,[†] Siddharth Somasundaram,[†] Khalifa M. Azizur-Rahman,[‡] Benjamin S. Williams,[†#] and Diana L. Huffaker[†‡#]

[†] Department of Electrical and Computer Engineering, University of California, Los Angeles, Los Angeles, California 90095, United States

[‡] School of Physics and Astronomy, Cardiff University, Cardiff, Wales CF24 3AA, United Kingdom

[#] California NanoSystems Institute, University of California, Los Angeles, Los Angeles, California 90095, United States

Abstract

In this work, we demonstrate an InAs nanowire photodetector at short-wavelength infrared (SWIR) composed of vertically oriented selective-area InAs nanowire photoabsorber arrays on InP substrates, forming InAs-InP heterojunctions. We measure a rectification ratio greater than 300 at room temperature, which indicates a desirable diode performance. The dark current density, normalized to the area of nanowire heterojunctions, is 130 mA/cm^2 at a temperature of 300 K and a reverse bias of 0.5 V, making it comparable to the state-of-the-art bulk InAs *p-i-n* photodiodes. An analysis of the Arrhenius plot of the dark current at reverse bias yields an activation energy of 175 meV from 190 K to 300 K, suggesting that the Shockley-Read-Hall (SRH) nonradiative current is the primary contributor to the dark current. By using three-dimensional electrical simulations, we determine that the SRH nonradiative current originates from the acceptor-like surface traps at the nanowire-passivation heterointerfaces. The spectral response at room temperature is also measured, with a clear photodetection signature observed at wavelengths up to 2.5 µm. This study provides an understanding of dark current for small bandgap selective-area nanowires and paves the way to integrate these improved nanostructured photoabsorbers on large bandgap substrates for high-performance photodetectors at SWIR.

Keywords

Nanowires, InAs, InP, SWIR, photodetector, heterojunction, dark current

III-V photodetectors operating at short-wavelength infrared (SWIR) wavelengths, i.e., between 1.4 – 3.0 μm, are sensors of choice for a broad range of applications, such as remote sensing, deep space imaging, and spectroscopy. These devices require high detectivity and low noise; however, compared with detectors working at wavelengths below 2.0 μm, their room-temperature operation commonly suffers from high dark current due to significant generation-recombination (G-R) and minority carrier diffusion current in small bandgap materials.[1,2] To address this issue, we propose reducing the volume of the SWIR photoabsorbers and integrating them on large bandgap materials to develop photodiodes with *p-n* heterojunctions. Such modifications drastically reduce minority carriers on either side of the junction, which leads to a suppression of G-R and minority carrier diffusion current, and consequently allows a much lower reverse biased dark current. These modifications can be accomplished by developing device schemes based on bottom-up vertical III-V nanowires. The unique properties of nanowires, namely small junction area and heteroepitaxy, are particularly advantageous in not only achieving lower dark current density, but also preventing threading dislocations (by elastic deformation at the nanowire-substrate heterointerfaces) and minimizing point dislocations, which are undesirable in the traditional epitaxy for planar structures.[3,4]

Great progress has been made recently for direct integration of vertical SWIR nanowire photoabsorbers on large bandgap materials. Examples of some pioneering studies include (1) single *n*-InAs nanowire on *p*-Si for photodetection at 1470 nm;[5] (2) *n*-InAs nanowire arrays on *p*-Si for wavelengths spanning up to 3 μm;[6] (3) *n*-InAs nanowire arrays on *n*-Si for a wavelength range covering 1.4 – 3.0 μm;[7] (4) unintentionally doped *n*-InAsSb nanowires on *p*-InAs (grown on GaAs substrate), giving a photoresponse up to 3.5 μm;[8] and (5) InAsSb *p-i-n* nanowire arrays on *p*-Si offering photoresponse up to ~3 μm.[9] However, a thorough analysis of the G-R mechanisms at reverse bias and a cross-comparison of its dark current with those of planar devices has not yet been performed. Note that the dark current in a three-dimensional (3-D) nanowire−substrate *p-n* diode with a heterointerface is predominantly determined by the heterointerface quality and the nanowire-air (or nanowire-passivation) interface quality around the nanowire depletion region. Therefore, the carrier dynamics in nanowires are more complicated than in

planar devices,[3,10] which needs to be thoroughly considered when developing high-performance nanowire based optoelectronic devices.

In this work, we present the electrical and optical properties of an InAs-InP heterojunction nanowire photodetector at SWIR, which is composed of vertically oriented, *n*-InAs nanowire photoabsorber arrays grown on *p*-InP substrates with selective area epitaxy. The nanowires are passivated with *in-situ* InP shell layers (~ 5 nm) to reduce nonradiative recombination centers on the surfaces.[11] These InAs-InP photodiodes with *p-n* heterojunctions exhibit a room-temperature rectification ratio greater than 300 and photodetection at wavelengths up to 2.5 μm. To compare the dark current of our devices with the state-of-the-art InAs *p-i-n* diodes, we normalized the measured dark current values to the active area of the InAs-InP nanowire heterojunctions, rather than the area of the nanowire array.[12] We observed nearly identical dark current density. To further understand the dark current mechanism, we applied a 3-D computational model to fit temperature-dependent current-voltage (I-V) curves and extract heterointerface and surface properties. The resultant simulations indicate that the suppression of dark current, via reduction of absorption volume and implementation of *p-n* heterojunctions, was offset by an increase in surface leakage current on the nanowire sidewalls. Finally, we showed the feasibility of achieving high detectivity by using the nanowire InAs-InP heterojunction platform to break the trade-off between high responsivity and low dark current. This study provides an understanding of dark current for small bandgap selective-area nanowires, and paves the way to integrate these nanostructured photoabsorbers on large bandgap substrates for high-performance photodetectors at SWIR.

Nanowire epitaxy and fabrication. The nanowires were grown by selective-area metal-organic chemical vapor deposition (SA-MOCVD). The substrate was a Zn-doped 2-inch on-axis InP (111)B wafer. We choose InP as the large bandgap substrate because it is feasible to achieve dislocation-free InAs-InP heterointerface for nanowire diameters up to 100 – 120 nm due to its modest lattice mismatch of 3.2%.[13] InAs-Si or InAs-GaAs heterojunctions suffer larger mismatches of 11.6% and 7.2% respectively. A 2D triangular lattice with nanohole diameter of 40 nm and pitch of 400 nm was patterned on a ~20 nm SiO_2

mask layer, atop an InP substrate, to promote selective area InAs nanowire growth. The overall size of the nanowire array was 100 μm × 100 μm, containing a total of 72,000 nanowires. The gaseous precursors during MOCVD growth were trimethylindium (TMIn), tertiarybutylarsine (TBAs), and tertiarybutylphosphine (TBP). Prior to the growth of the InAs nanowire segment (V/III ratio of 8), a thin InAs seeding layer (V/III ratio of 32) was introduced as a buffer to assist nucleation along the (111)B orientation and avoid formation of any twin boundaries along the (111)A orientation.[14,15] InAs nanowires were unintentionally *n*-doped and were *in-situ* passivated by InP shells (intrinsic, thickness of ~ 5 nm, V/III ratio of 8) to reduce nonradiative surface recombination centers on the nanowire sidewalls.[11] The as-grown nanowires have a diameter of 100 nm (without the InP passivation shells) and a height of 1.4 µm. A scanning electron microscope (SEM) image of the nanowire array with high vertical yield and high uniformity is shown in Figure 1a. More details of the InAs nanowire growth are provided in the Supporting Information (SI.1).

Following the growth, the nanowires were planarized using benzocyclobutene (BCB), an electrically insulating filler medium between the nanowires that supports the top contact and isolates it from the bottom. Vias to the InP substrate were defined by photolithography. The BCB film was then cured at 250°C for 60 minutes and an Au (20 nm)/Zn (20 nm)/Au (200 nm) film was deposited on the substrate to define the bottom p-contact. Then, the BCB film was etched back using reactive ion etching process to expose ~400 nm of the nanowire tip, followed by a 15-second selective HCl:H_2O (1:2) chemical etch of the InP passivation shells for top metal contacts. Next, a Cr (10 nm)/Au (150 nm) film was deposited atop the nanowire tips at a tilt angle of ~45° to form plasmonic gratings that would strongly couple incident light on surface plasmon resonance. Schematics of the device structure are illustrated in Figure 1b and a SEM image of the self-aligned plasmonic couplers are shown in Figure 1c. The spectral response measurement was then conducted by packaging the fabricated InAs photodetector array on a 68-pin leadless chip carrier through wire bonding, as shown in Figure 1d.

Diode analysis. Temperature-dependent I-V characterization of the device from 100 K to 300 K were carried out using a Lakeshore PS-100 cryogenic probe station, as shown in Figure 2a. We observe a rectification ratio greater than 300 at 300 K and greater than 2000 at 100 K (at 1 V, both forward and reverse biased). We then compare the dark current level of our devices with that of planar InAs *p-i-n* photodiodes (working in photovoltaic mode at room temperature, grown by either MOCVD or molecular beam epitaxy) as a means for quantifying the dark current of our device.[2,16,17] For planar photodiodes, the dark current level is quantified as dark current density, $J_{Dark\_J} = I_{Dark}/A_J$, where I_{Dark} is the measured dark current and A_J is the area of the etched homojunction or heterojunction mesa. However, nanowire photodiodes with nanowire-substrate *p-n* heterojunctions do not have an easily defined device (or effective) area A_{Eff}, which poses a challenge in efficiently comparing nanowire and planar devices.[12] As a result, to make a fair comparison, we normalize the dark current to the junction area of the *n*-InAs/*p*-InP photodiodes instead. Since the depletion regions extend from the bottom nanowire segments, the total junction area is the sum of the area of all x-y cross-sections of the nanowires. In other words, $A_J = N \times A_{NW}$, where N is the total number of nanowires in an array and A_{NW} is the x-y cross-sectional area of a single nanowire.

As mentioned earlier, the photodetector array is composed of 72000 nanowires, and the average diameter (edge-to-edge, without InP passivation layers) of each nanowire is 100 nm (± 5 nm). With this information, we calculate the dark current density J_{Dark_J} of our nanowire array at 300 K and a reverse bias of 0.5 V to be about 130 mA/cm^2. Then, we compare our calculated J_{Dark_J} with that of the best commercial and research InAs *p-i-n* photodetectors, including photovoltaic detectors, avalanche photodetectors, and photodiodes, in similar characterization conditions (at 300 K and at a reverse bias of 0.5 V), as shown in Figure 2b.[2,16,17] Note that we simply use the mesa area as A_J when calculating the dark current density for the compared planar devices. The average J_{Dark_J} of the abovementioned planar devices is 123 mA/cm^2, marginally lower than the dark current level of our *n*-InAs/*p*-InP photodiodes.

Here, we provide further analysis to better understand the source of the dark current level of the InAs nanowire photodiodes. There are two critical factors that enable low dark current density: (1) significant

suppression of minority carrier diffusion, and (2) high quality of InAs-InP heterointerfaces. The first factor can be simply interpreted by the saturation current density equation for a heterojunction given by[18]

$$J_0 \equiv q\left(\frac{D_{p1}}{L_{p1}N_{D1}}n_{i1}^2 + \frac{D_{n2}}{L_{n2}N_{A2}}n_{i2}^2\right), \quad (1)$$

where D is the diffusivity of the minority carriers, L is the diffusion length, N is the impurity concentration, n_i is the intrinsic carrier concentration, and the subscripts 1 and 2 refer to two different materials. For the InAs nanowire photodiodes, materials 1 and 2 are n-type InAs and p-type InP respectively. Our approach is to achieve low J_0 by reducing n_{i1} by significantly reducing n-type volume (InAs nanowire) and n_{i2} using a large bandgap substrate, i.e., InP instead of InAs. Regarding the second factor, nanowire heteroepitaxy allows for a dislocation-free heterointerface, as the diameter of the nanoholes is only 40 nm. The thin-film heteroepitaxy technique, on the other hand, cannot achieve such heterointerface, as the large lattice mismatch and difference in thermal expansion coefficient between the two materials will inevitably cause the formation of high-density threading dislocations and point dislocations. Note that since the heterointerfaces are located within the active p-n junctions, any local defects within the heterointerfaces can contribute to nonradiative recombination and leakage current, which significantly degrade the photodetector performance.

Based on the explanation in the previous paragraph, we expect that $J_{\text{Dark\_J}}$ of the nanowire device should be even lower than the values reported for thin-film InAs p-i-n devices.[2,16,17] Note that the bandgap of InAs nanowires is 0.442 eV, different from the bulk zinc-blende (ZB) InAs bandgap of 0.365 eV at 300 K (further discussion on the significance of this will be provided in the next section). Thus, the intrinsic carrier concentration of the InAs nanowires, given by n_{i1} in Eq. 1, is lower than that of ZB InAs, and therefore is expected to have less contribution to the dark current. We note that the dark current of the nanowire device (at 300 K) shows a strong dependence on the applied voltage when reverse biased, having a two-order increase from 0.1 V to 1.0 V. At such low biases, field sensitive current generation mechanisms such as trap-assisted tunneling and avalanching are not likely to be the contributors to the dark current.

Rather, the increase in dark current can be attributed to the surface leakage on the nanowire sidewalls between the InAs nanowire cores and InP passivation shells. With increasing reverse bias, the heterojunction extends further into the InAs nanowire segments, meaning that a larger surface area will be depleted and further contribute to the dark current. This is not surprising because the performance of nanowire-based devices is predominantly affected by the surface leakage due to the large surface-to-volume ratios of the nanowires.

To determine whether the surface leakage can account for the bias-dependent increase of dark current, we perform further analysis of temperature-dependent I-V curves by extracting the activation energy at reverse biases of 0.2 V, 0.5 V, and 1.0 V and temperatures from 170 K to 300 K using the following exponential relationship

$$I_{Dark} \propto T^{3/2} \exp\left(\frac{-E_A}{k_B T}\right) \tag{2}$$

where I_{Dark} is the dark current, T is the temperature, E_{A} is activation energy, and k_{B} is the Boltzmann constant. The resultant activation energies for the given temperature and bias values are consistently between 0.173 eV and 0.175 eV, as shown in Figure 3. Typically, the Fermi-level of a bare InAs nanowire without surface passivation is pinned above its conduction band due to its large surface state density. However, by adding InP passivation layers, the Fermi level lowers toward the midgap (hovering about 0.046 – 0.048 eV above it), indicating a significant reduction of surface states.

To further quantify I_{Dark} of InAs nanowire photodiodes, we perform 3-D electrical simulation (in Synopsys Sentaurus TCAD) to fit the I-V curves (in Figure 2a) and extract InAs nanowire surface properties. To achieve this, we simulate a unit cell of a nanowire array that comprises of two InAs nanowires (with InP passivation shells for each), a dielectric growth mask (SiO_2), a growth substrate (InP), and ambient air, as schematically shown in Figure 4a. The dimensions of the simulated nanowires are defined from measuring the dimensions of the actual nanowires from the SEM measurements. Note that the 3-D metal top contacts are defined on the exposed nanowire segments to mimic the actual fabricated device

with plasmonic gratings. In the electrical model, the effects of Shockley-Read-Hall (SRH) nonradiative recombination are introduced into the nanowire-passivation (*n*-InAs/*i*-InP) interface, the nanowire-substrate (*n*-InAs/*p*-InP) interface, and the nanowire-air interface. The local trap capture and emission model (surface trap model) is applied to the InAs-InP nanowire-passivation heterointerfaces, described by the equation[18]

$$R_{Trap} = \frac{N_t v_{th}^p v_{th}^n \sigma_p \sigma_n (np - n_i^2)}{v_{th}^p \sigma_p (p + p_1) + v_{th}^n \sigma_n (n + n_1)} \tag{3}$$

with

$$p_1 = n_i exp\left(\frac{-E_t}{k_B T}\right) \tag{4}$$

and

$$n_1 = n_i exp\left(\frac{E_t}{k_B T}\right) \tag{5}$$

where N_t is the trap density (in cm^{-2}), v_{th} is the thermal velocity (in cm s^{-1}), σ is the trap cross section (in cm^2), and E_t is the trap energy, or the energy difference between the trap state and midgap state (in eV). In the simulations, E_t is kept fixed at 0.75 eV while N_t varies as a fitting parameter. The carrier traps are specified as acceptor-like surface traps (neutral when unoccupied and negtively charged when occupied by electrons). For nanowire-substrate (*n*-InAs/*p*-InP), nanowire-air (*n*-InAs/vacuum) and nanowire-mask (n-InAs/SiO_2) interfaces, we introduce surface recombination velocities instead of trap states to reproduce the nonradiative recombination mechanisms, as shown in previous studies for heterointerfaces.[3] Finally, the simulated dark current of one unit cell is multiplied by 36000 (the number of unit cells within the 100 μm × 100 μm nanowire array) to find the total dark current produced by the nanowire array. A summary of the material parameters used in the simulations can be found in the Supporting Information SI.2.

Figure 4b shows the simulated I-V curves at 190 K and 300 K with and without the surface trap model. The fitted N_t at the nanowire-passivation (InAs-InP) heterointerfaces is 2×10^{12} cm^2. It becomes immediately clear that the simulated dark current of nanowires with surface traps has a strong dependence

on bias. Without surface traps, the dark current is mostly attributed to the minority carrier diffusion and depletion layer G-R. Note that the simulated dark current without surface traps is almost constant at higher biases (> 0.2 V) because the contribution from saturation current (i.e. minority carrier diffusion from *n*-InAs nanowires) is much greater than from G-R within depletion regions. Figure 4c shows cross-sectional views of the electric field profiles at reverse biases of 0.2 V, 0.5 V, and 1.0 V, along with a line cut along the *x*-axis near the bottom of the nanowire. Initially, the electric field is confined between the nanohole and the bottom segment of BCB. As the bias is increased, the depletion region edge extends upwards toward the middle of the nanowire segment and BCB layer. During this process, the electric field at nanowire-passivation heterointerfaces builds up, resulting in larger drift velocity of dark carriers towards the sidewalls. Note that the high field region (where the electric field is greater than 4×10^4 V/cm) in the nanowire segment is relatively small, meaning that avalanching is unlikely to occur.

Optical characterizations. Photoluminescence (PL) of as-grown InAs nanowires with InP passivation layers is carried out by a solid-state red laser at 671 nm and a liquid-nitrogen cooled InSb detector in a Thermo Scientific Nicolet 6700 Fourier-transform infrared (FTIR) spectrometer. Spectral response of the wire-bonded detector array is measured using an infrared source in the FTIR spectrometer, an attached Thermo Scientific Nicolet Continuum microscope (equipped with a liquid-nitrogen cooled MCT-A detector and a Nexus detector interface box), and a Stanford SR570 preamplifier. The details regarding the normalization of the spectral response are given in the Supporting Information SI.3.[8]

Figure 5a shows room-temperature PL emission of the InAs nanowire photodiode array (before device fabrication) and simulated optical absorption of the fabricated device. PL emission is clearly observed, which suggests that a significant reduction of surface state density of InAs nanowires was achieved by introducing large bandgap phosphorus-based *in-situ* passivation layers.[14] Detailed studies of In(As)P passivation on InAs nanowires have been previously reported, showing significant enhancement of PL emission at different temperatures.[19-22] In addition, we also observe in a previous study that the PL emission from InAs(Sb) inserts in InAsP nanowires was drastically enhanced when *in-situ* InAsP

passivation layers were implemented.[23] It is well known that by introducing phosphorus into InAs, the surface state density can be largely suppressed (a strong room-temperature PL emission from arsenic-rich InAsP nanowires is shown in this study). Note that the measured optical emission peak at 2.8 μm indicates a calculated bandgap of 0.442 eV, which differs from the theoretical ZB InAs bandgap of 0.364 eV (all values are at 300 K). This is primarily due to a high density of rotational twins, i.e., crystal phase switches between ZB and wurtzite (WZ), which is more commonly observed in InAs nanowires grown by selective-area vapor-solid (VS) growth technique.[11,23] Such high density is not as common in nanowires grown by gold-catalyst vapor-liquid-solid (VLS) growth mode without intentional switching of growth conditions for InAs(ZB)-InAs(WZ) heterostructures.[24-26] Electromagnetic simulations are performed to estimate the absorptance within the nanowires. The triangular nanowire lattice (with pitch of 400 nm) and diameter (of 100 nm) used in this fabrication was originally optimized to excite a surface plasmon polariton at approximately 1.5 μm operation, which can be seen from the enhanced simulated absorption peak (> 8%) shown in Figure 5a, hence the absorption is estimated to be lower than 2% at wavelengths longer than 2.0 μm.[8] In future works, an optimized nanowire-plasmonic structure could be applied to excite surface plasmon polariton resonance over 2.0 μm for achieving high optical absorption and quantum efficiency.

Figure 5b shows the calibrated responsivity of the InAs nanowire photodiode array at 300 K (at a reverse bias of 0.5 V), with photodetection achieved at wavelengths up to 2.5 μm. The inset depicts the calculated external quantum efficiency (EQE). To the best of our knowledge, this is the first reported room-temperature responsivity over 2 μm for InAs nanowire photodetectors. The responsivity at 77 K has significantly less noise than at 300 K due to lower dark current, showing a similar responsivity profile (Supporting Information SI.4). Note that the calibrated responsivity and EQE are relatively low compared to the planar InAs *p-i-n* diodes. In addition, the spectral response at 0 V is too weak to be resolved. The low responsivity, or EQE, is due to the exclusive generation of photogenerated carriers within the top segments of the nanowires near the plasmonic gratings. This first leads to a loss of these carriers through nonradiative recombination at the nanowire-passivation (InAs-InP) heterointerfaces due to a high density of surface trap

states. Secondly, since the entire nanowires are unintentionally *n*-doped and no junctions are formed at nanowire tips, there is no electric field to properly drift the photogenerated carriers to the 3-D contacts. This currently limits the operation of our nanowire photodiode in photovoltaic mode. Therefore, introducing a highly doped *n*-type region at the nanowire tips can potentially enhance the responsivity of our structure in photovoltaic mode.

The calculated detectivity (D^*) at a reverse bias of 0.5 V is shown in Figure 6, which is calculated based on the responsivity spectrum shown in Figure 5b and the following well-known equation (assuming that the nanowire photodiode works in a quantum-limited regime)

$$D^* \approx \frac{R}{\sqrt{2qJ_{Dark\_Eff}}} \tag{6}$$

where R is the responsivity, $J_{\text{Dark\_Eff}}$ is the dark current density, and q is the electron charge. Note that the interpretation of $J_{\text{Dark\_Eff}}$ here differs from that of the aforementioned dark current density $J_{\text{Dark\_J}}$. Here, $J_{\text{Dark\_Eff}} = I_{\text{Dark}}/A_{\text{Eff}}$, where A_{Eff} represents the area of the nanowire array (100 μm × 100 μm). The peak detectivity at SWIR is close to 2.5×10^7 cm·Hz$^{1/2}$/W, which is two orders lower than that of commercial InAs *p-i-n* photodiodes (photovoltaic ~ 0 V). This lower level of detectivity is mainly due to a lower quantum efficiency (i.e. optical absorption and internal quantum efficiency) and can be further increased by improving passivation quality and tuning the geometrical structure of the nanowire device to enhance absorption via surface plasmon resonance.[8,27]

Toward high-detectivity InAs-InP heterojunction photodiodes. The purpose of this work is to show that the nanowire platform with nanoscale photoabsorbers and InAs-InP heterojunctions has the potential to provide performance improvements for D^*. There exists a fundamental limit to achieve higher D^* due to the trade-off between high R and low $J_{\text{Dark\_Eff}}$ in planar devices, as shown in Eq. 6. In this work, we have reduced the effective dark current density $J_{\text{Dark\_Eff}}$ by reducing photoabsorption volume using the nanowire material system. We obtain identical dark current density compared to a bulk photodiode (normalized to the nanowire cross-sections) with a fill-factor of about 4%, which suggests a 5-fold decrease

of $J_{Dark\_Eff}^{1/2}$, bypassing the negative impact from the additional surface area of the nanowires. This is not only due to the reduction of the fill factor to reduce the G-R volume, but also by usage of InAs-InP heterojunctions to significantly reduce the number of minority carriers. However, this was achieved at the expense of reduced absorption and responsivity R, leading to a net lowering of D^*.

The next challenge then is clearly how to increase R and further reduce J_{Dark_Eff} to obtain a net improvement in D^* for nanowire photodetectors. First, it is necessary to develop a better surface passivation because of the high trap density currently observed at InAs-InP (nanowire-passivation) interfaces. Based on the simulations shown in Figure 4b, it is also possible to reduce J_{Dark_Eff} by one order, i.e., a 3-fold decrease of $J_{Dark\_Eff}^{1/2}$. Thus, an over 15-fold decrease of $J_{Dark\_Eff}^{1/2}$ is expected. Second, the nanowire pattern and the plasmonic grating can be optimized to maximize the optical absorption at SWIR by varying the nanowire pitch and diameter to achieve same order of magnitude absorption as that of planar thin-film devices.[8,27] Third, the internal quantum efficiency can be improved by introducing a highly doped layer atop the InAs nanowire segment, creating an intrinsic electric field that would sweep the carriers to the contact. As a result, although the absorption of planar InAs *p-i-n* photodiodes (~70%) is roughly 7 times higher than that of the nanowire-based InAs photodetectors, we can still potentially achieve 15-fold reduction in $J_{Dark\_Eff}^{1/2}$, effectively breaking the trade-off between high R and low J_{Dark_Eff}.

In summary, we developed InAs nanowire photodiodes on InP substrates for photodetection at SWIR. The photodiodes were comprised of nanostructured photoabsorbers and *n*-InAs/*p*-InP (nanowire-substrate) *p-n* heterojunctions. I-V characteristics showed a rectification ratio of over two orders at room temperature, suggesting a desirable diode performance. The dark current density at a reverse bias of 0.5 V, normalized to the junction area, was comparable to that of the best commercial or research InAs *p-i-n* photodiodes. This is because the dark current of *n*-InAs/*p*-InP photodiodes was drastically suppressed by decreased photoabsorber volume, which reduced minority carrier diffusion from *p*-type materials, and passivation with *in-situ* InP shells. In addition, the electrical simulations showed that the bias dependent performance was strongly influenced by the surface leakage on nanowire sidewalls. Finally, the spectral

response at room temperature was measured, showing a clear photodetection signature at SWIR. We also discussed the feasibility of achieving high D^* by using the nanowire InAs-InP heterojunction platform to break the trade-off between high responsivity and low dark current. Further work can be carried out to improve nanowire surface quality and optimize optical design for higher detectivity at room temperature. This work paves the way to integrate nanostructured photoabsorbers at SWIR on large bandgap substrates to achieve comparable detection performance metrics as their planar counterparts.

ASSOCIATED CONTENT

Supporting Information

The Supporting Information is available free of charge on the ACS Publications website at http://pubs.acs.org.

Detailed information about the nanowire growth, materials parameters used in the electrical simulations, details regarding the normalization of spectral response, more characterizations at 77 K.

AUTHOR INFORMATION

Corresponding Author

*Email: dingkun.ren@ucla.edu

ORCID

Dingkun Ren: 0000-0001-9470-1956

Xiao Meng: 0000-0002-7061-9840

Alan C. Farrell: 0000-0001-6083-9121

Benjamin S. Williams: 0000-0002-6241-8336

Notes

The authors declare no competing financial interest.

ACKNOWLEDGMENTS

We gratefully acknowledge the support from the National Science Foundation (grant no. ECCS-1509801) and the Air Force Office of Scientific Research (grant no. FA9550-15-1-0324). In addition, the authors would like to acknowledge the financial support provided by Sêr Cymru National Research Network in Advanced Engineering and Materials.

REFERENCES

(1) InGaAs photodiodes.

Available online: https://www.hamamatsu.com/resources/pdf/ssd/ingaas_kird0005e.pdf.

(2) InAs photovoltaic detectors (P10090-01).

Available online: https://www.hamamatsu.com/resources/pdf/ssd/p10090-01_etc_kird1099e.pdf.

(3) Ren, D.; Scofield, A. C.; Farrell, A. C.; Rong, Z.; Haddad, M. A.; Laghumavarapu, R. B.; Liang, B.; Huffaker, D. L. *Nanoscale* **2018**, 10 (16), 7792-7802.

(4) Dick, K. A.; Caroff, P. *Nanoscale* **2014**, 6 (6), 3006-3021.

(5) Brenneis, A.; Overbeck, J.; Treu, J.; Hertenberger, S.; Morkötter, S.; Döblinger, M.; Finley, J. J.; Abstreiter, G.; Koblmüller, G.; Holleitner, A. W. *ACS Nano* **2015**, 9 (10), 9849-9858.

(6) Wei, W.; Bao, X.-Y.; Soci, C.; Ding, Y.; Wang, Z.-L.; Wang, D. *Nano Lett.* **2009**, 9 (8), 2926-2934.

(7) Wook Shin, H.; Jun Lee, S.; Gun Kim, D.; Bae, M.-H.; Heo, J.; Jin Choi, K.; Jun Choi, W.; Choe, J.-w.; Cheol Shin, J. *Sci. Rep.* **2015**, 5, 10764.

(8) Lee, W.-J.; Senanayake, P.; Farrell, A. C.; Lin, A.; Hung, C.-H.; Huffaker, D. L. *Nano Lett.* **2016**, 16 (1), 199-204.

(9) Thompson, M. D.; Alhodaib, A.; Craig, A. P.; Robson, A.; Aziz, A.; Krier, A.; Svensson, J.; Wernersson, L.-E.; Sanchez, A. M.; Marshall, A. R. J. *Nano Lett.* **2016**, 16 (1), 182-187.

(10) Ren, D.; Rong, Z.; Somasundaram, S.; Azizur-Rahman, K. M.; Liang, B.; Huffaker, D. L. (*Nanotechnology, under review*).

(11) Lin, A.; Shapiro, J. N.; Scofield, A. C.; Liang, B. L.; Huffaker, D. L. *Appl. Phys. Lett.* **2013**, 102 (5), 053115.

(12) Farrell, A. C.; Senanayake, P.; Meng, X.; Hsieh, N. Y.; Huffaker, D. L. *Nano Lett.* **2017**, 17 (4), 2420-2425.

(13) Glas, F. *Phys. Rev. B* **2006**, 74 (12), 121302.

(14) Ren, D.; Farrell, A. C.; Williams, B. S.; Huffaker, D. L. *Nanoscale* **2017**, 9 (24), 8220-8228.

(15) Ren, D.; Farrell, A. C.; Huffaker, D. L. *MRS Adv.* **2017**, 2 (58-59), 3565-3570.

(16) Sun, W.; Lu, Z.; Zheng, X.; Campbell, J. C.; Maddox, S. J.; Nair, H. P.; Bank, S. R. *IEEE J. Quantum Electron.* **2013**, 49 (2), 154-161.

(17) Zhou, X.; Meng, X.; Krysa, A. B.; Willmott, J. R.; Ng, J. S.; Tan, C. H. *IEEE Sens. J.* **2015**, 15 (10), 5555-5560.

(18) Sze, S. M.; Ng, K. K. Physics of Semiconductor Devices, 3rd ed.; John Wiley & Sons, 2006.

(19) Jurczak, P.; Zhang, Y.; Wu, J.; Sanchez, A. M.; Aagesen, M.; Liu, H. *Nano Lett.* **2017**, 17 (6), 3629-3633.

(20) van Tilburg, J. W. W.; Algra, R. E.; Immink, W. G. G.; Verheijen, M.; Bakkers, E. P. A. M.; Kouwenhoven, L. P. *Semicond. Sci. Technol.* **2010**, 25 (2), 024011.

(21) Treu, J.; Bormann, M.; Schmeiduch, H.; Döblinger, M.; Morkötter, S.; Matich, S.; Wiecha, P.; Saller, K.; Mayer, B.; Bichler, M.; Amann, M.-C.; Finley, J. J.; Abstreiter, G.; Koblmüller, G. *Nano Lett.* **2013**, 13 (12), 6070-6077.

(22) Choi, C. H.; Kim, H. D.; Lee, R.; Shin, J. C.; Kim, D. G.; Kim, J. S. *Curr. Appl. Phys.* **2017**, 17 (12), 1742-1746.

(23) Ren, D.; Farrell, A. C.; Huffaker, D. L. *Opt. Mater. Express* **2018**, 8 (4), 1075-1081.

(24) Dick, K. A.; Thelander, C.; Samuelson, L.; Caroff, P. *Nano Lett.* **2010**, 10 (9), 3494-3499.

(25) Thelander, C.; Caroff, P.; Plissard, S.; Dey, A. W.; Dick, K. A. *Nano Lett.* **2011**, 11 (6), 2424-2429.

(26) Yan, X.; Li, B.; Zhang, X.; Ren, X. *Appl. Surf. Sci.* **2018,** 458, 269-272.

(27) Ren, D.; Rong, Z.; Azizur-Rahman, K. M.; Somasundaram S.; Huffaker, D. L. (*to be submitted*, *Nanotechnology*)

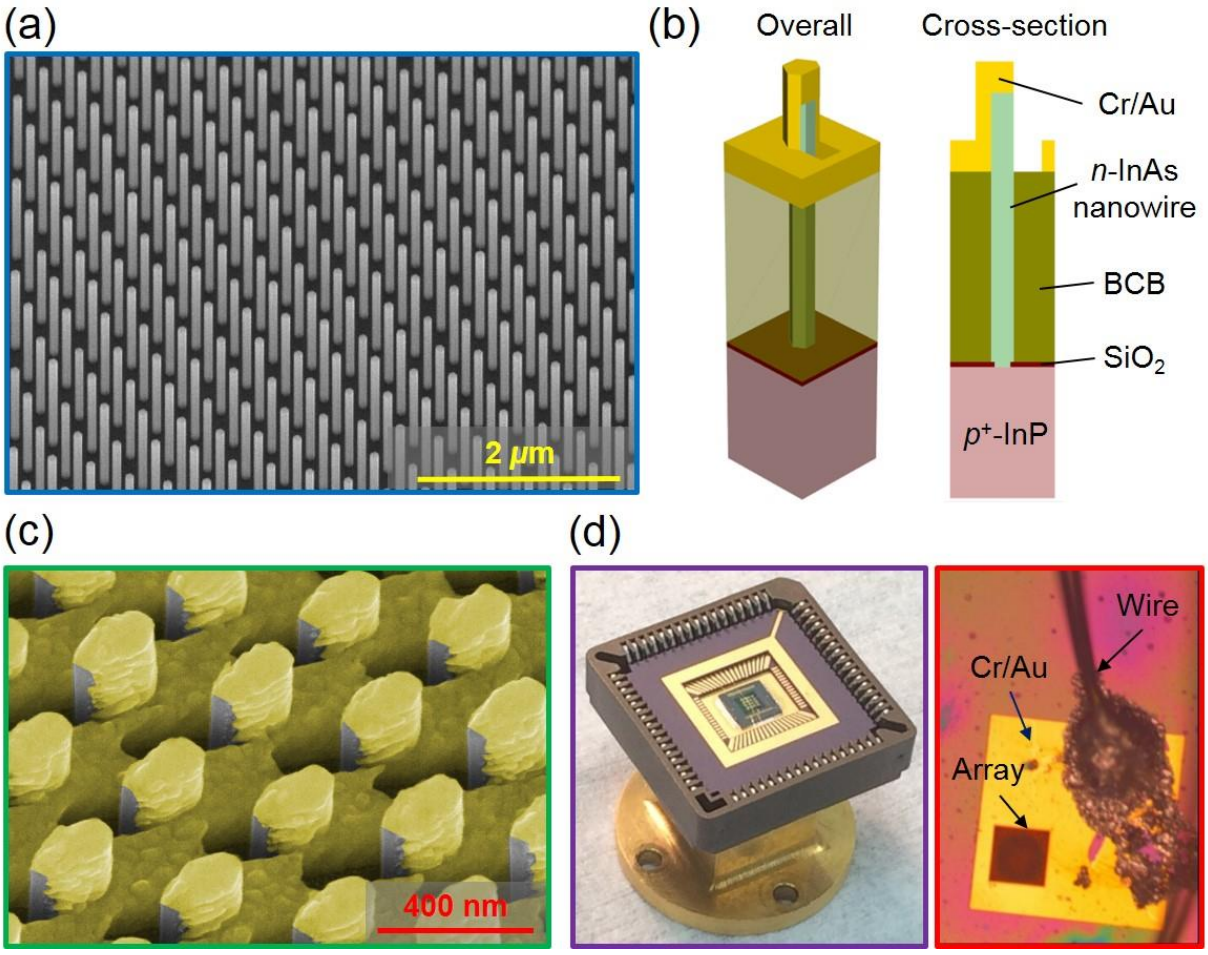

Figure 1. (a) As-grown InAs nanowire arrays on InP (111)B substrate. (b) Schematics of the unit cell of an InAs nanowire photodetector (InP passivation layer is not shown). (c) Close-up view of plasmonic gratings. (d) Wire-bonded photodetector device sample (left). (d) Close-up view of the wire-bonded nanowire array (right). The size of the array is 100 μm × 100 μm.

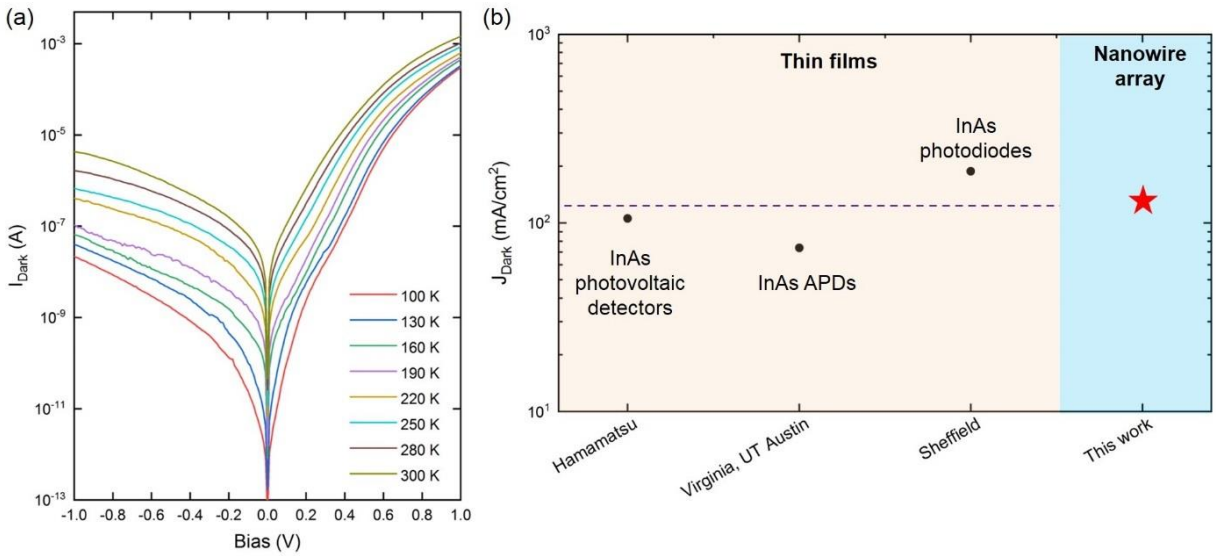

Figure 2. (a) Temperature-dependent I-V characteristics of InAs-InP photodiodes with nanowire-substrate *p*-*n* heterojunctions. (b) Comparison of room-temperature dark current density at a reverse bias of 0.5 V between the nanowire photodetector and the best commercial or research InAs homojunctions. The model of Hamamatsu uncooled InAs photovoltaic detector is P10090-01. The dark current of the InAs nanowire array is normalized by the junction area of the *n*-InAs/*p*-InP heterointerfaces (i.e., *n*-InAs nanowire cross-section A_J), not by the area of nanowire array (A_{Eff}).

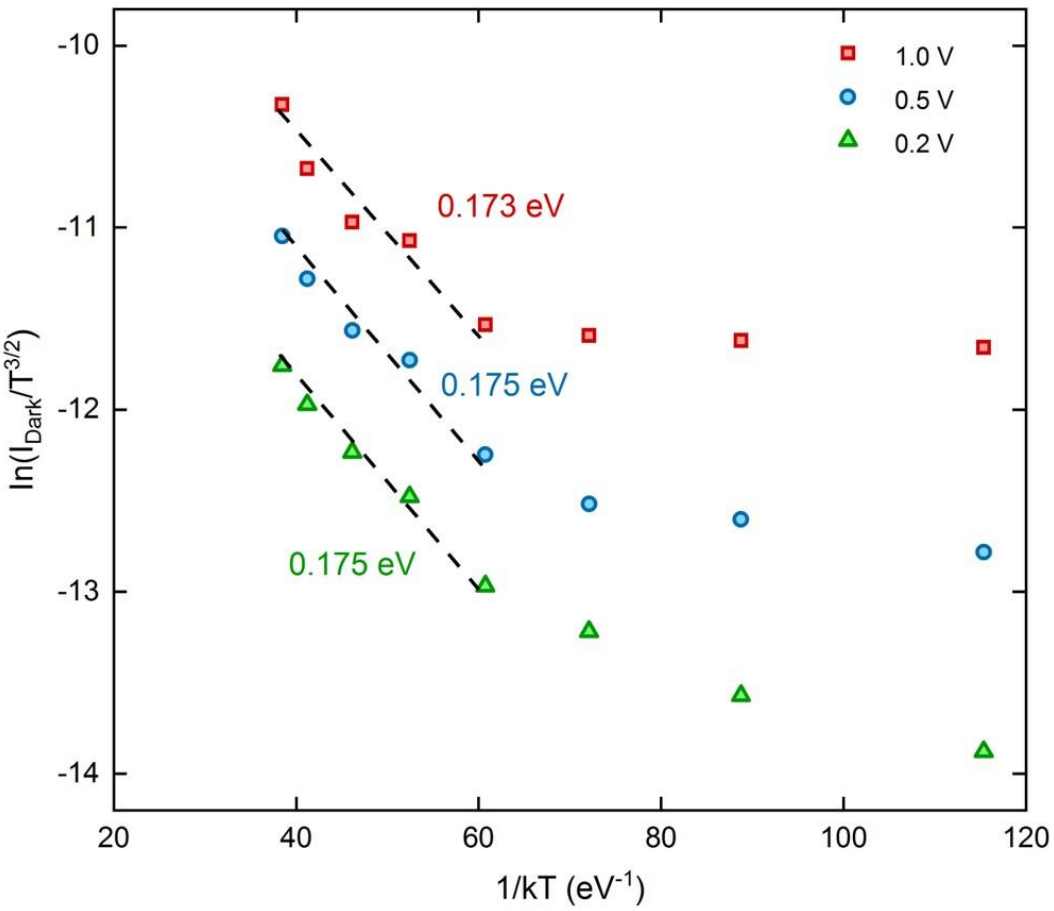

Figure 3. Arrhenius plot of the measured current at reverse biases of 0.2 V, 0.5 V, and 1.0 V. Extracted values of activation energy are labeled.

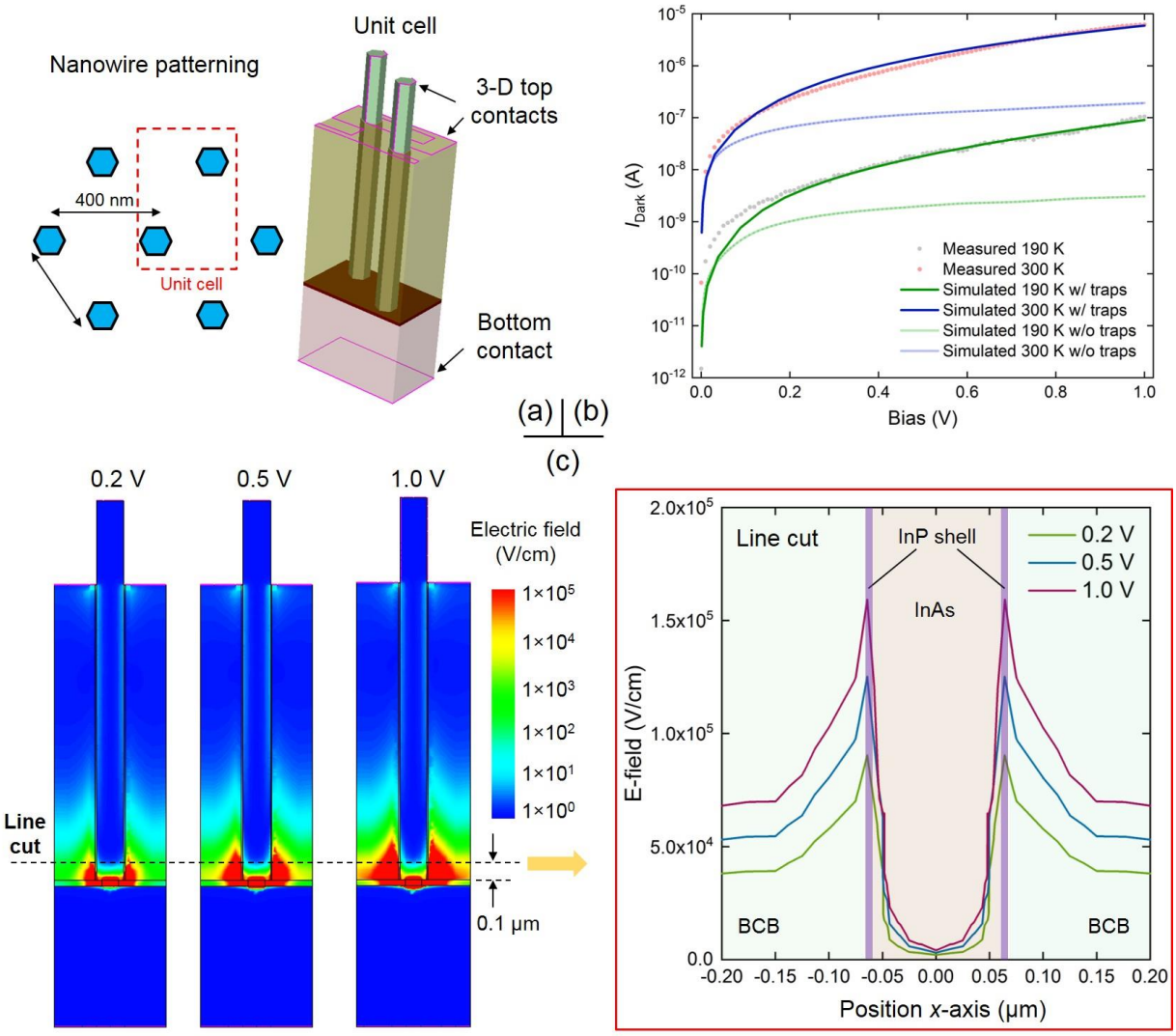

Figure 4. (a) Schematics of a unit cell in the electrical model. (b) Comparison of simulated and measured dark current (reverse biased) at 190 K and 300 K, both with and without the surface trap model. (c) Left: cross-sectional mapping of simulated electric field distributions at reverse biases of 0.2 V, 0.5 V, and 1.0 V. Right: line cut of electric field profiles along the *x*-axis (region labeled in (c)).

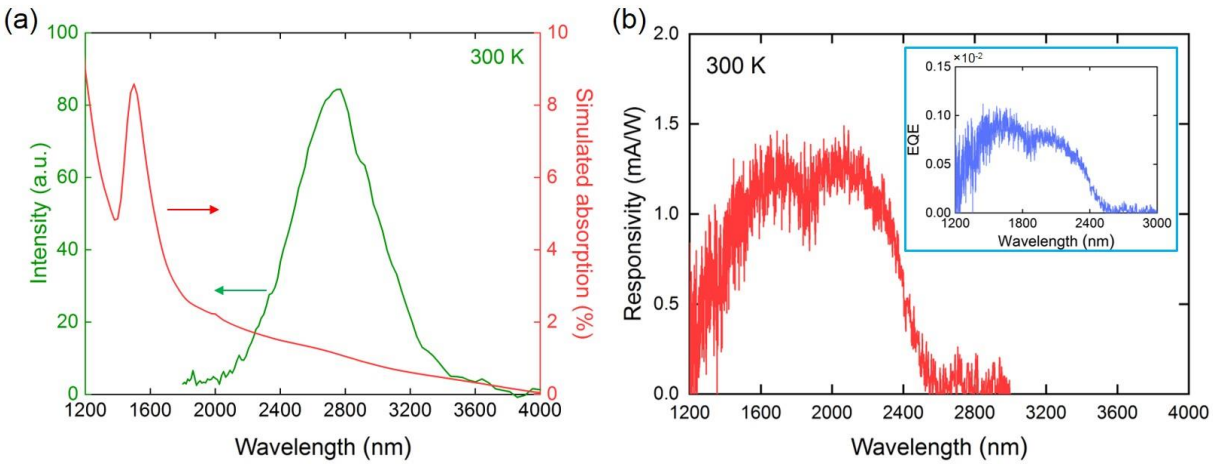

Figure 5. Optical characterizations of *n*-InAs/*p*-InP photodiode at 300 K. (a) PL of as-grown InAs-nanowires with InP passivation layers (left *x*-axis) and simulated optical absorption (right *y*-axis). (b) Spectral response of the InAs photodetector at reverse bias of 0.5 V, indicating photodetection signature at SWIR up to 2.5 µm. The inset shows the calculated EQE in fractions.

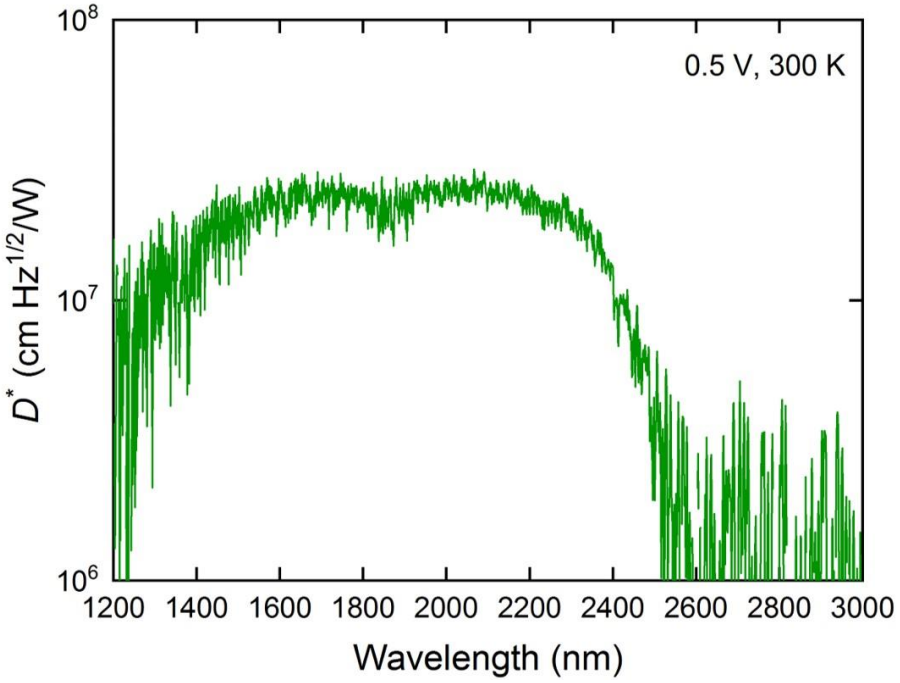

Figure 6. Detectivity (D^*) spectrum of n-InAs/p-InP photodiode at 300 K (at reverse bias of 0.5 V).

TABLE OF CONTENTS